Journal of Digital Imaging (2018) 31:912–922
https://doi.org/10.1007/s10278-018-0075-x

Pattern Recognition and Size Prediction of Microcalcification Based on Physical Characteristics by Using Digital Mammogram Images

G. R. Jothilakshmi[1] · Arun Raaza[2] · V. Rajendran[1] · Y. Sreenivasa Varma[3] · R. Guru Nirmal Raj[4]

Published online: 5 June 2018

Abstract
Breast cancer is one of the life-threatening cancers occurring in women. In recent years, from the surveys provided by various medical organizations, it has become clear that the mortality rate of females is increasing owing to the late detection of breast cancer. Therefore, an automated algorithm is needed to identify the early occurrence of microcalcification, which would assist radiologists and physicians in reducing the false predictions via image processing techniques. In this work, we propose a new algorithm to detect the pattern of a microcalcification by calculating its physical characteristics. The considered physical characteristics are the reflection coefficient and mass density of the binned digital mammogram image. The calculation of physical characteristics doubly confirms the presence of malignant microcalcification. Subsequently, by interpolating the physical characteristics via thresholding and mapping techniques, a three-dimensional (3D) projection of the region of interest (RoI) is obtained in terms of the distance in millimeter. The size of a microcalcification is determined using this 3D-projected view. This algorithm is verified with 100 abnormal mammogram images showing microcalcification and 10 normal mammogram images. In addition to the size calculation, the proposed algorithm acts as a good classifier that is used to classify the considered input image as normal or abnormal with the help of only two physical characteristics. This proposed algorithm exhibits a classification accuracy of 99%.

Keywords Digital mammogram · Microcalcification · Pattern recognition · Binning · Reflection coefficient · Mass density · 3D interpolation · Size calculation of microcalcification

Introduction

Breast cancer is one of the major common cancers affecting women in both developed and developing countries. Because an approach to prevent breast cancer has not yet been found, early detection is important to decrease the mortality [1]. The yearly increase in the incidence of breast cancer can be understood from the alarming reports given by various health organizations such as the World Health Organization (WHO) and American Cancer Society (ACS). The World Cancer Research Fund (WCRF) International had projected the cancer cases worldwide as 12.7 million by 2008, and it has predicted the number to rise to 21 million by 2030. Figure 1 shows the estimated age-standardized incidence and mortality rates of breast cancer globally as per the statistics of the ACS.

From the perspective of a physician, the major abnormalities related to breast are masses and calcifications. Masses [2, 3] are not much vulnerable compared with calcifications. Calcification can be further classified as macro and microcalcification. Macrocalcifications [4] are large calcium deposits in the breast tissue, formed owing to aging. However, minute calcium

✉ G. R. Jothilakshmi
jothi.se@velsuniv.ac.in

Arun Raaza
arunraaza@gmail.com

V. Rajendran
hodece@velsuniv.ac.in

Y. Sreenivasa Varma
drysvarma@gmail.com

R. Guru Nirmal Raj
gurunirmal2010@gmail.com

[1] Department of ECE, Vels University, Chennai, India

[2] Vels University, Chennai, India

[3] Varma Nursing Home and Research Center, Pallikaranai, Chennai, India

[4] Department of ECE, Lakshmiammal Polytechnique College, Kovilpatti, Tamil Nadu, India

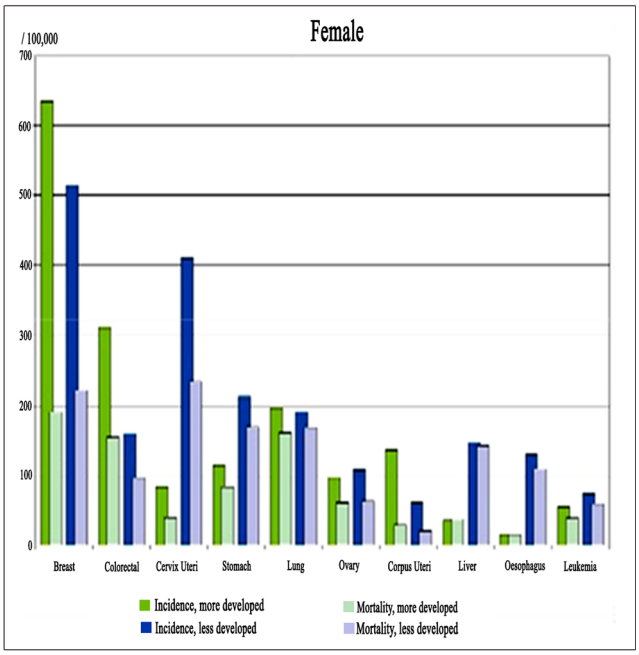

Fig. 1 Incidence and mortality statistics of the most common cancers worldwide

deposits in the breast tissue lead to the most vulnerable form of cancer called microcalcifications. Both masses and microcalcifications are further categorized as benign and malignant [5] based on their size, shape, and margins. Malignant cancers are dangerous compared with benign cancers.

Various image processing techniques are useful for the detection of microcalcification [6, 7] and classification of cancer as benign and malignant using textural and shape features. A wide literature survey reveals that the conventional approach for detecting and classifying microcalcification involves enhancement [8, 9], followed by segmentation [10, 11], feature extraction [12], and classification [13]. In general, X-ray mammograms [14], sonograms [15], computed tomography [16], and magnetic resonance imaging [17] are the tools used for detecting breast cancer. X-rays are considered as a prime screening technique to detect breast abnormalities, particularly breast cancer. It is a non-invasive procedure with the advantage of a low cost, time effectiveness, and good resolution. The advancement of pattern recognition [18] and image processing techniques needs to be introduced in a user-friendly manner to assist a physician in readily providing the important required advice to the patients regarding the problem areas. This paper proposes a combination of pattern recognition of a phenomenon related to microcalcification and an advanced image processing technique to present a user-friendly method to a clinical doctor. The proposed method uses a new concept to measure the size of the microcalcification region by a calculation of the physical characteristics of the identified pattern of the microcalcification. To obtain the physical characteristics of the lesion part in the digital mammogram, initially, the input image is binned. Binning is a technique that divides the images into sub-regions, and it is particularly useful to move closer to the lesion part and further perform the analysis only with the selected sub-region. The binning concept is highly useful to analyze underwater images [19, 20], and in this work, this borrowed concept is used for the first time to examine medical imaging to measure the size of a microcalcification region. Moreover, the calculation of the reflection coefficient of a digital mammogram image and mass density using image processing technique is a unique method that is followed in this work.

Description and Classification of Image Information

As mentioned in the "Introduction," we have specifically taken diagnostic digital mammogram images for identifying the occurrence of microcalcification. A digital mammogram is the best method to detect a cancerous zone in the breast [21]. A small deposit of calcium distributed in a certain way that may turn into cancer is defined as microcalcification. Microcalcification is classified into benign and malignant in terms of its size, shape, margins, and distribution, and the presence of calcium radicals. Calcium oxalate is related to benign cancers, whereas calcium phosphate is associated with malignant cancers. It has been reported in the literature that microcalcification is one of the prime elements that might cause certain clinical problems in women. Its early detection and user-friendly representation to physicians would be highly useful for analyzing its size, shape, and spread of the radicals (calcium oxalate/phosphate). In a diagnostic digital mammogram, microcalcification appears as bright white spots. The intensity associated with microcalcification is higher than that of the other regions in the breast. It is mandatory to identify the region of interest (RoI) by segregating it from the background. This could be achieved by using image processing techniques to detect the lesion part from the fatty tissue. The pattern recognition of the lesion portion is a vital part for the further analysis and classification of the abnormalities occurring in breasts.

Pattern Recognition

A pattern recognition technique is useful for classifying the characteristics of images based on the similarities in certain features [22]. To identify a pattern related with a lesion, its associated characteristics associated need to be determined. Generally, various segmentation techniques are used to identify the RoI. A preprocessing technique for image enhancement is applied using the min–max [23], median [23], Weiner [23], and Volterra filters [24]. Conventional mammograms are noisy, low contrast, and blurred images. Mammogram enhancement is necessary to highlight specific features of images. During segmentation, thresholding- [25], boundary- [26], and region-based [27] methods are used. Segmentation in image processing plays a central role in detection of the RoI

from the background. From the RoI, statistical features [28] are extracted, and by using SVM [29], fuzzy k-means [26], and C-means [30] clustering, the identified pattern is classified.

Materials and Methods

The proposed method is useful to detect the pattern of a microcalcification image, which is different from the conventional pattern recognition methods. Here, the pattern of a microcalcification is found from its physical characteristics. The considered physical characteristics are the reflection coefficient and mass density [31–34] of lesion part in digital mammogram images. The detected microcalcification pattern is projected as 3D image to find the size of microcalcification. The proposed flow consists of nine steps, which are explained in detail as follows.

(i) Image acquisition: The digital mammogram images are obtained from the digital database for screening mammography (DDSM) [35, 36]. They contain normal and abnormal mammogram images. Benign and cancer (malignant) images have been reported in the abnormal image category. Malignant images are downloaded and used for this research work. Hundred images are selected from the DDSM, each with the dimension of 768 × 512, i.e., each image has 768 rows and 512 columns. Each image size is measured in terms of the distance (height and width) as 5.38 × 4.6 in inches or 136.6 × 116.8 in millimeter. Figure 2 shows the difference between a normal mammogram and a mammogram with malignant microcalcification. The intensities associated with the abnormal region are high, which is highlighted by a red circle, whereas the clustered microcalcification appears as bright white spots within the RoI.

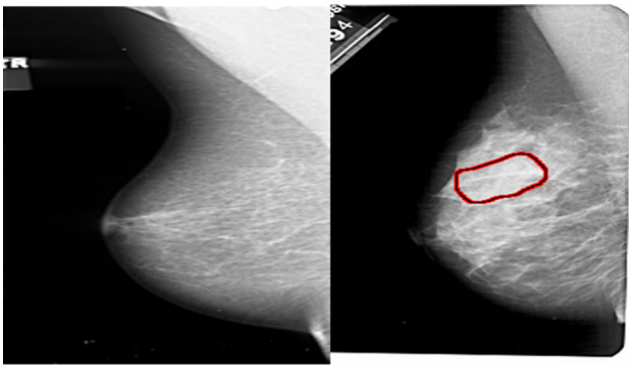

(a) (b)

Fig. 2 **a** Normal mammogram. **b** Malignant mammogram

(ii) Image binning: The entire mammogram image is binned initially with three rows and four columns. The criteria for choosing the matrix size of the bins are as follows:

1. To obtain equal-sized bins
2. If the entire mammogram is binned with more number of rows and columns, the size of the individual bin and its matrix size reduce. As per characteristics of a microcalcification, it may be distributed into more than one bin. Therefore, in second-level binning, to obtain the size of the microcalcification, more than one bin needs to be analyzed.
3. If the entire mammogram is binned with few rows and columns, the size of the individual bin and its matrix become large. Therefore, an unwanted background may be present along with microcalcification. Therefore, a first-level binning with three rows and four columns is suitable for further analysis.

In first-level binning, each bin presents its own matrix of 256 × 128. They are represented in terms of distance as 46 × 29 mm. The bin, which contains the RoI, is identified and again subjected to further binning with two rows and two columns. In the second-level binning, each bin has its own matrix of 128 × 64 (refer to Figs. 14 and 17), and it is represented in terms of the distance as 23 × 15 mm (refer to Fig. 18).

(iii) Calculation of reflection coefficient:

A breast consists of soft and fatty tissues. In these tissues, a solid tumor is formed by calcium deposits. When a breast with such an abnormality is exposed to an X-ray source, the solid lesion part reflects the energy. Accordingly, it is possible to calculate the reflection coefficient for the whole image including the lesion part. In the lesion part, the reflected energy and reflection coefficient are both high. An image could be modeled as a two-dimensional function f(x,y) with two components as

$$f(x,y) = i(x,y)\, r(x,y)$$

where i(x,y) is the illumination component and r(x,y) is the reflectance component.

$$0 < i(x,y) < \infty$$
$$0 < r(x,y) < 1$$

When $r = 0$, it represents total absorption, and when $r = 1$, it represents total reflectance.

(iv) Calculating range of reflection coefficient through least square curve fitting:

In second-level binning, after selecting the appropriate bin with the lesion region, to segment the RoI, it is mandatory to determine the range of the reflection coefficient to serve as the threshold. To this end, the reflection coefficient graph for each row is plotted by considering the corresponding bin column number in the x axis and the minimum to maximum range of the reflection coefficient in the y axis. For the bin consisting of the RoI, it is possible to plot 128 reflection coefficient graphs (refer to Figs. 6, 7, 8, and 9 with red line). The exact range of the reflection coefficient that serves as the threshold for the RoI is found by applying least square curve fitting (refer to Figs. 6, 7, 8, and 9 with blue line) because the variation is very rapid. By analyzing this plot for 100 images with respect to the lesion part, the range of the reflection coefficient was found by using least square curve fitting. Least square curve fitting consists of raw data and a function with unknown coefficients. It is necessary for identifying the coefficients value in such a way that the raw data matches that of the function. Coefficient values that are the "best" suited are the ones that lower the overall chi-square value. The following equation defines the chi-square:

$$\sum_i \left(\frac{y-y_i}{\sigma_i}\right)^2$$

y Fitted value of the given point,

y_i The value pertaining to the measured data for the point, and

σ_i Estimate of the standard deviation of Y_i.

The range of the reflection coefficient for all the four second-level bins is found (refer to Table 1), and the range related to the RoI is 0.9 to 1.

(v) Segmenting RoI by thresholding with respect to range of reflection coefficient

The RoI is segmented by the combination of the range of the reflection coefficient as the threshold and using exact mapping. By the former, the segmented image of a lesion is obtained (refer to Fig. 12). Subsequently, the complement of the segmented image is obtained and merged with the selected second-level bin to yield the RoI exactly along with the boundary of the lesion (refer to Fig. 13). Thus, by using thresholding and exact mapping, the RoI is exactly segmented, which is available in either as a single bin or a combination of appropriate bins in second-level binning.

(vi) Calculation of mass density:

The basic definition of mass density is mass/volume. Because the lesion part consists of a hard calcium deposit, it is possible to find the mass density of the affected portion. Microcalcification occurs owing to the deposition of calcium radicals such as calcium oxalate and calcium phosphate. Benign calcifications are composed of calcium oxalate [31], whereas malignant

Table 1 Calculation of the reflection coefficient, mass density, and size of the microcalcification

Sl. no.	Image no.	Reflection coefficient				Mass density(g/cm^3)				Microcalcification size in mm
		Bin 1 (1,1)	Bin 2 (1,2)	Bin 3 (2,1)	Bin 4 (2,2)	Bin 1 (1,1)	Bin 2 (1,2)	Bin 3 (2,1)	Bin 4 (2,2)	
Abnormal images (malignant microcalcification)										
1	Image 1-6-(1,1)	0.9–1	0.6–0.7	0.2–0.3	0.6–0.7	2.8726	2.5762	2.7249	2.6914	5
2	Image 2-7-(1,1)	0.9–1	0.1–0.2	0.4–0.6	0.5–0.6	3.0011	2.9707	2.9692	2.7100	8
3	Image 3-8-(1,1)	*0.9–1*	*0.8–0.9*	*0.7–0.8*	*0.8–0.9*	*3.1777*	*3.0328*	*3.1661*	*3.1297*	*7*
4	Image 4-1-(1,2)	0.8–0.9	0.9–1	0.7–08	0.8–0.9	2.9115	2.9360	2.8871	2.9202	6
5	Image 5-2-(2,1)	0.7–0.9	0.6–0.7	0.9–1	0.4–0.5	1.2614	2.1492	2.9756	2.8989	7
6	Image 6-4-(1,2)	0.6–0.7	0.9–1	0.7–0.8	0.3–0.4	2.456	2.814	2.675	1.568	4
7	Image 7-5-(2,2)	0.7–0.8	0.5–0.6	0.8–0.9	0.9–1	1.984	2.319	2.634	3.108	5
8	Image 8-10-(2,2)	0.1–0.2	0.7–0.8	0.3–0.4	0.9–1	2.001	2.191	2.342	2.931	3
9	Image 9-3-(2,1)	0.6–0.7	0.8–0.9	0.9–1	0.8–0.9	2.729	2.545	2.872	3.125	0
10	Image 10-12-(1,2)	0.5–0.6	0.9–1	0.7–0.8	0.6–0.7	2.286	2.786	2.630	2.435	4
Normal type image										
11	Image 11-7	0.5–0.6	0.5–0.6	0.7–0.8	0.6–0.7	2.432	2.469	2.576	2.672	0
12	Image 12-6	0.4–0.5	0.6–0.7	0.9–1	0.5–0.6	1.950	2.413	2.722	2.677	0
13	Image 13-5	0.0–0.1	0.4–0.5	0.3–0.4	0.6–0.7	0.370	1.303	1.777	2.272	0
14	Image 14-6	0.3–0.4	0.8–0.9	0.5–0.6	0.7–0.8	2.1244	2.637	2.213	2.464	0
15	Image 15-6	0.5–0.6	0.4–0.5	0.6–0.7	0.5–0.6	2.363	2.367	2.690	2.544	0

The corresponding output values for the considered input image (Fig. 3), is shown in italics (Sl. no. 3)

calcifications are composed of calcium phosphate [32]. The mass density of calcium oxalate is 2.12 g/cm^3 [33] and that of calcium phosphate is 3.14 g/cm^3 [34]. The mass density of microcalcification is found by using the volume density comment in MATLAB. Here, the mass of the segmented RoI is found for the concerned second-level bin by calculating its corresponding volume. From these values, the mass density of the RoI is calculated. The calculated value of the mass density is listed in Table 1.

(vii) Mapping between reflection coefficient and mass density

The mass densities of all the four second-level bins are found (refer to Table 1), and the range of the mass density of the malignant microcalcification related to the RoI lies between 2.7 and 3.1 g/cm^3. Mapping the range of the reflection coefficient (0.9 to 1) to the mass density (2.7 to 3.1) is performed (refer to Fig. 10) to confirm the occurrence of microcalcification. Because the reflection coefficient and mass density are found to be based on the intensities of the pixels in the RoI, linear mapping between the reflection coefficient and mass density can take place.

(viii) Detecting the pattern of microcalcification and its projection as a 3D image:

Based on the calculated range of the reflection coefficient and mass density associated with the microcalcification, its pattern is detected in the binned image, and the extracted pattern is projected as 3D images by two methods.

1. Projecting the whole second-level bin consisting the microcalcification pattern, by considering the x and y axes in terms of the rows and columns of the second-level bin (128 × 64) and z axis in terms of the calculated range of the reflection coefficient (refer to Fig. 14).
2. Projecting the microcalcification alone in the RoI (i) by considering the x and y axes in terms of the rows and columns of the second-level bin (128 × 64) and z axis in terms of the calculated range of the reflection coefficient (refer to Fig. 17)

   and (ii) by considering the y and x axes in terms of the height and width of the considered second-level bin (23 × 15 mm) and z axis in terms of the reflection coefficient (refer to Fig. 18). It is also possible to rotate the 3D-projected image in any angle, which is very helpful for further clinical analysis by the physicians (refer to Figs. 15, 16, 19, and 20). Among these seven 3D projections, Figs. 14 and 18 play a vital role. Because Fig. 14 is used to cross-check the rows and columns of the second-level bin with the RoI, Fig. 18 is highly useful to measure the size of the microcalcification.

(ix) Interpolating the size of microcalcification:

Because the 3D vision of the binned image is projected with respect to the distance, using this algorithm, it is very easy to calculate the size of the microcalcification. In Fig. 18, the x and y axes represent the width and height of the selected second-level bin. The same figure includes a cluster of the microcalcification. In the cluster, a larger sized microcalcification is considered. Its horizontal extreme points are identified, and these points are projected with the x axis to yield the size of the microcalcification (refer to Table 1 with Sl. no. 3). The size of the microcalcification varies from millimeters to a few centimeters depending on the stage of the cancer.

Results and Discussion

Interpolation is the process of using known data to estimate values at an unknown location. Initially, it is not easy to exactly locate the microcalcification in the digital mammogram images visually. The image gives only the details of the intensities based on the nature of the breast tissue. When the acquired diagnostic mammogram image is converted into gray scale, the intensities vary from 0 to 255. Only with this available data and by calculating the reflection coefficient and mass density, it is possible to calculate the size of the malignant microcalcification using the projected 3D pattern. The results of the eight steps as mentioned above are shown below. Figure 3 is the considered input image. Figure 4 exhibits the three rows and columns after the first-level binning. It has 12 bins in total. These are numbered horizontally. The eighth bin

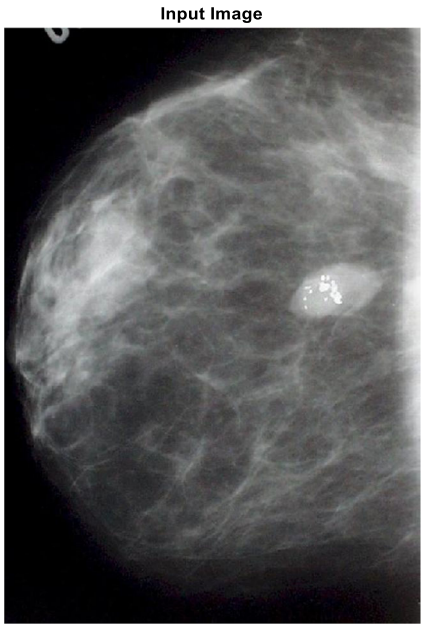

Fig. 3 Input mammogram with microcalcification

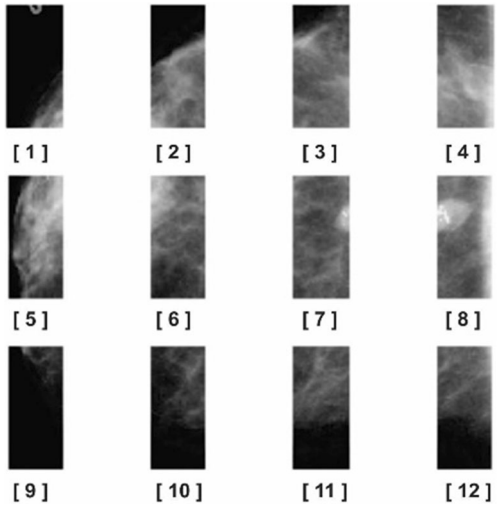

Fig. 4 First-level binning (bin 8 is subjected to second-level binning)

consists the lesion part (RoI). Therefore, it is subjected to second-level binning. It is represented by Fig. 5, where bin 1,1 includes the microcalcification clusters. It is selected for further analysis. It consists of a matrix of 128 × 64 size. The reflection coefficient is calculated for all the pixels associated with bin 1,1. Then, the variation in the reflection coefficients is plotted for each row, as in Figs. 6, 7, 8, and 9. From these plots, it is understandable that the reflection coefficient starts to vary between 0.9 and 1 from row 66 until row 112. The actual rapid variation of the reflection coefficient is

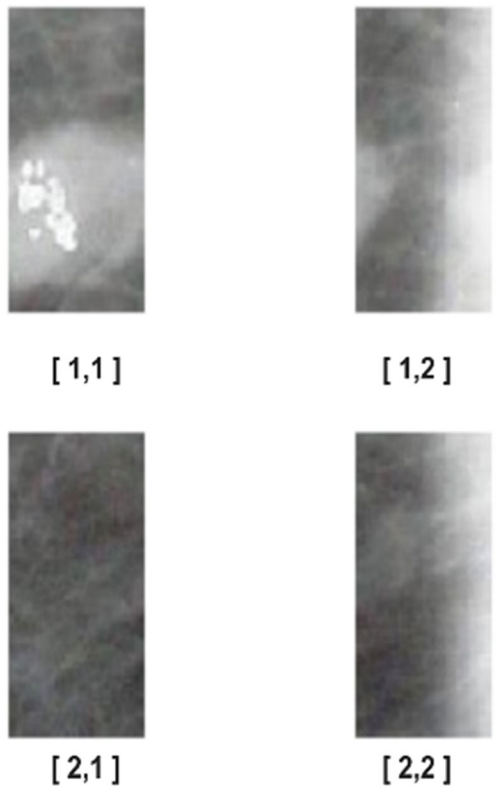

Fig. 5 Second-level binning–numbering 1,1; 1,2; 2,1; 2,2 horizontally

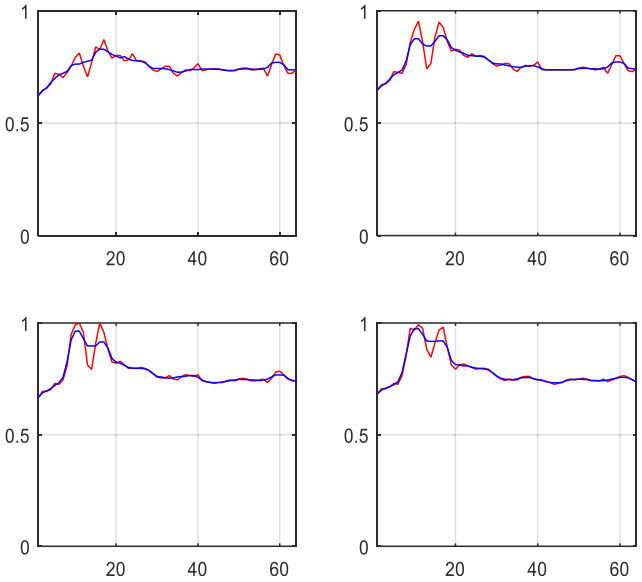

Fig. 6 Reflection coefficient plot for bin 1,1 with row nos. 65–68

highlighted by a red line, and the range of the reflection coefficient associated with the RoI found by using least square curve fitting is represented by a blue line. The least square curve fitting smoothens the wide variations in the RoI. Figure 10 shows the linear variation of the range of reflection coefficient and mass densities. Figure 11 represents the values of the mass densities in all the four second-level bins, and according to this plot and Table 1, bin 1,1 has the highest mass density. Figure 12 displays the segmented RoI by considering the range of the reflection coefficient as the threshold, and Fig. 13 presents the exact RoI by mapping Fig. 12 with bin 1,1. Figures 14, 15, 16, 17, 18, 19, and 20 display the 3D projections of the microcalcification patterns, which are useful

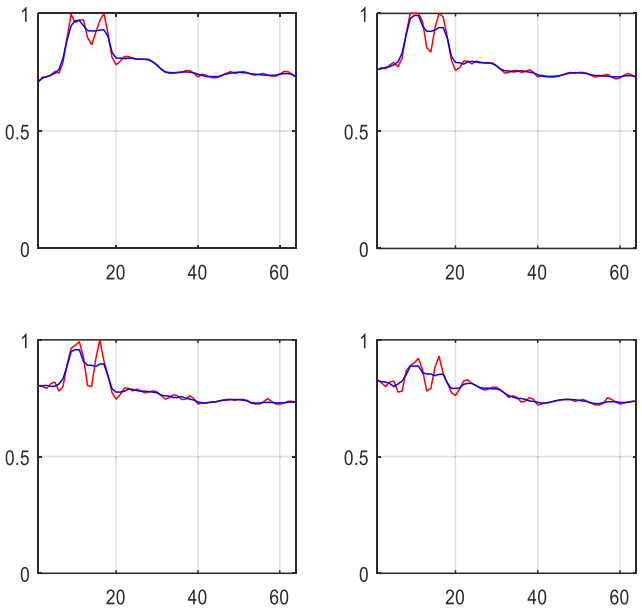

Fig. 7 Reflection coefficient plot for bin 1,1 with row nos. 69–72

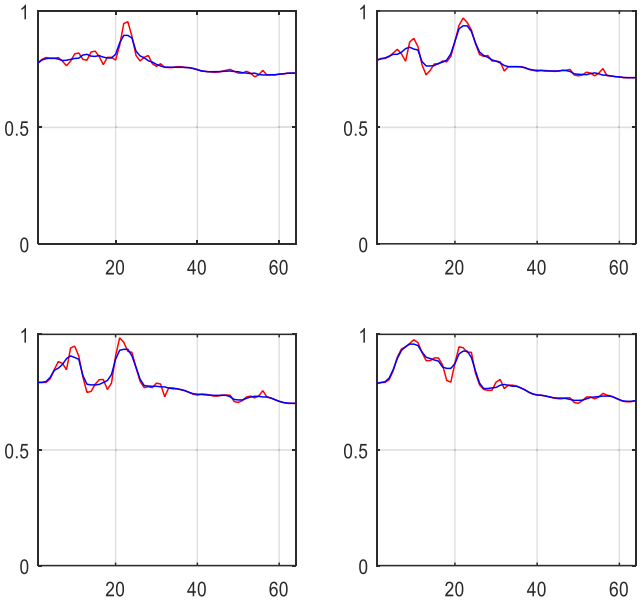

Fig. 8 Reflection coefficient plot for bin 1,1 with row nos. 73–76

to predict their characteristics. Figure 18 shows a cluster of microcalcification, where three small closed regions are noted. Out of the three, the first one (one that is projected horizontally) is comparatively larger than the other two. Therefore, it is mapped with the x axis, and its size is found as 7 mm (refer to Table 1 in Sl. no. 3).

Quantitative Assessment on Mammograms

Based on the above flow of the proposed methodology, the value for the reflection coefficients, mass densities of the second-level bins, and microcalcification size are calculated with 100 abnormal images. However, the above-mentioned values are tabulated only for 10 samples with malignant microcalcifications and 5 samples with normal mammograms

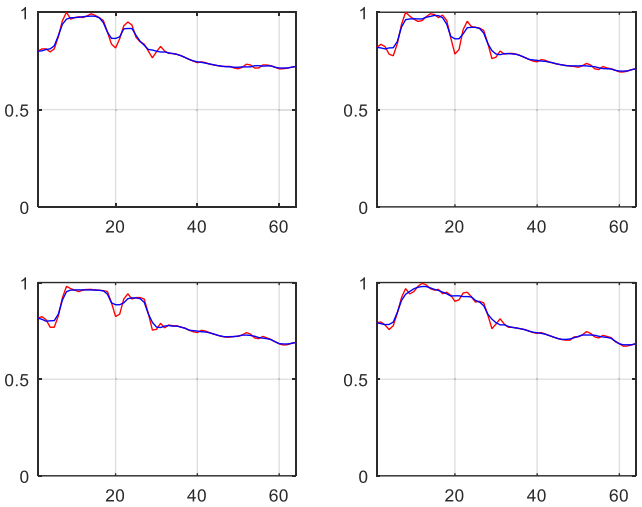

Fig. 9 Reflection coefficient plot for bin 1,1 with row nos. 77–80

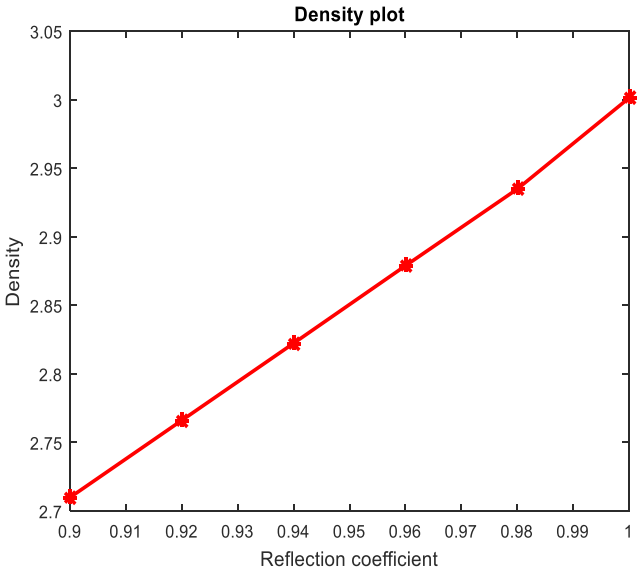

Fig. 10 Reflection coefficient and mass density mapping

in Table 1. Table 1 consists of four major columns, namely, image number, reflection coefficient, mass density, and size of microcalcification. The image number column gives information about

- The image with the corresponding number considered for the analysis
- The bin number of the first-level binning where the lesion is found
- The bin number(s) of the second-level binning where the lesion is found.

In this paper, the output figures are corresponding to Sl. no. 3 in Table 1, where the image number is mentioned as 3-8-(1,1), i.e., image 3 is considered for the analysis and in the first-level binning, the lesion is found in eighth bin (8). In the second-level binning, the affected region is available in the

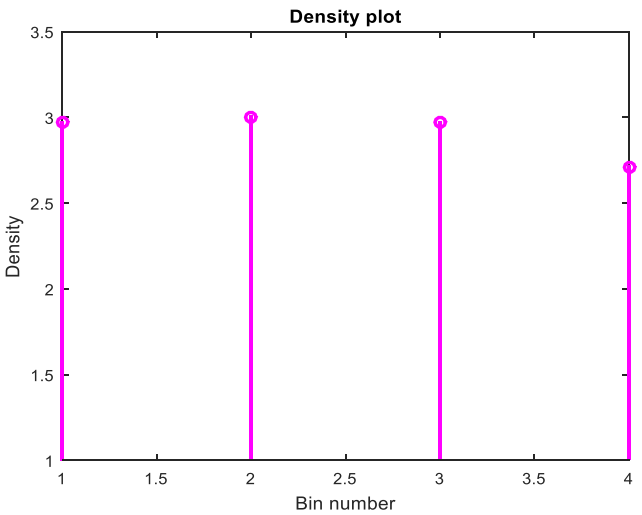

Fig. 11 Density calculation of second-level bins

Fig. 12 Identifying the RoI by thresholding

first bin (1,1). Then, in the reflection coefficient column, the reflection coefficients of the four second-level bins are calculated and listed. Similarly, in mass density column, the mass densities of the four second-level bins are given. Then, the size of the maximized calcification is given in millimeter (mm).

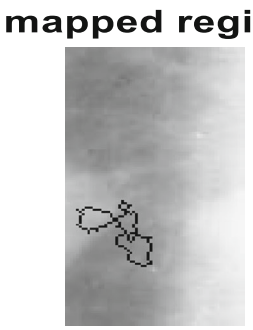

Fig. 13 Exact RoI by mapping

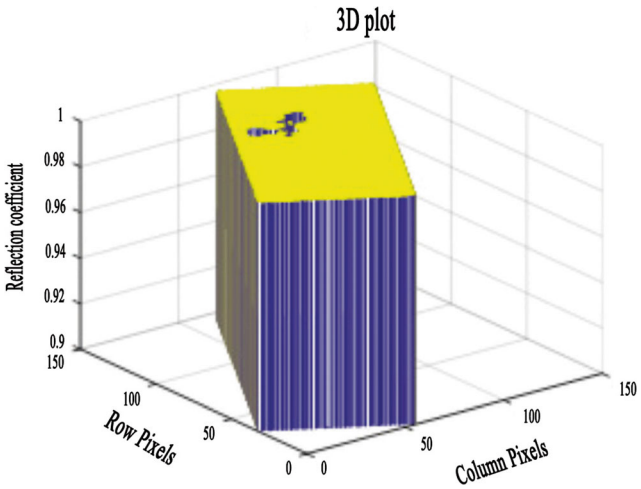

Fig. 15 Microcalcification pattern for bin 1,1 with 30° rotation

In this study, 100 abnormal images with malignant microcalcification and 10 normal images are considered for the analysis. The prediction class for each image is found and listed in Table 2. Using the obtained prediction class, we can calculate the accuracy, which is described in terms of true positive, true negative, false negative, and false positive, which are as follows:

True positive (TP) = 99

True Negative (TN) = 10

False Positive (FP) = 0

False Negative (FN) = 1

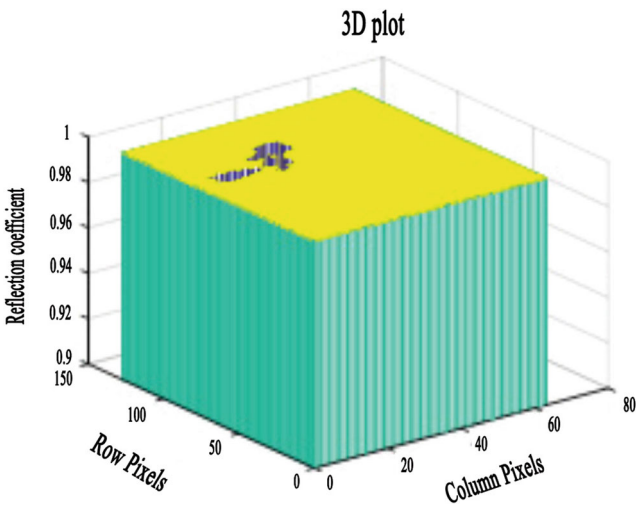

Fig. 14 Detection of the microcalcification pattern for bin 1,1

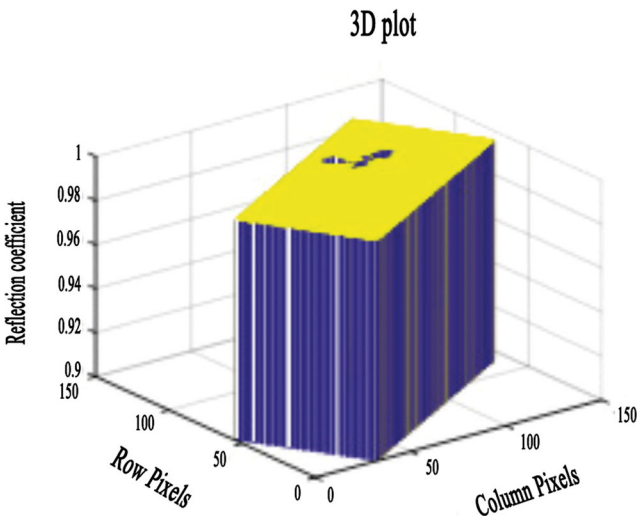

Fig. 16 Microcalcification pattern for bin 1,1 with 60° rotation

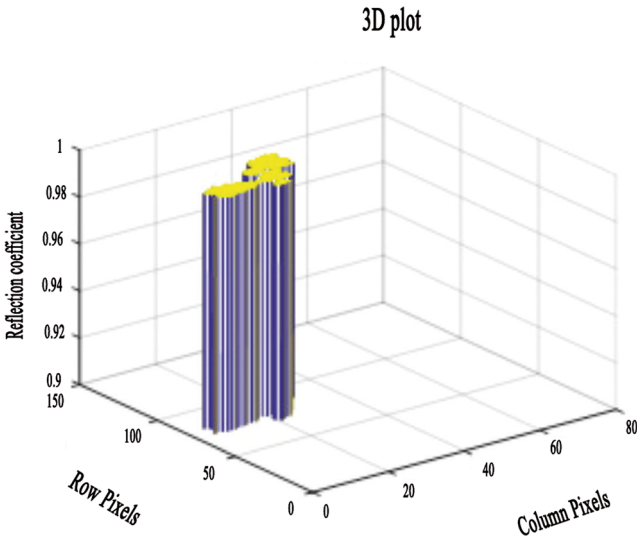

Fig. 17 3D view of projected microcalcification alone

$$\text{Accuracy} = \frac{\text{Number of correct assessments}}{\text{Number of all assessments}}$$

Prediction class accuracy

$$= (\text{TN} + \text{TP})/(\text{TN} + \text{TP} + \text{FN} + \text{FP}) \quad = 0.990\ (99\%)$$

Discussion

From the data of Table 1, it is clearly understood that when the reflection coefficient and mass density of the considered bin lie in the prescribed range, then, it is possible to predict the size of the microcalcification accurately. If we consider the data associated with Sl. no. 3, the RoI is in bin number (1,1) and its reflection coefficient lies between 0.9 and 1 and mass density lies between 2.7 and 3.1 g/cm^3. For the remaining bins, the reflection coefficients do not fall within the prescribed range, but their mass densities lie within the prescribed range. Therefore, the algorithm selects bin (1,1) as the RoI and not the remaining three bins. However, in Sl. no. 9, we consider an image with an abnormality, and the RoI is found in (2,1). Even though, the reflection coefficient and mass density fall in the prescribed range, the size of the microcalcification could not be found. Therefore, it falls in the false negative category. This may be owing to the considered breast that may contain denser tissues. A similar flow is followed in the normal mammograms, and all the considered images fall in

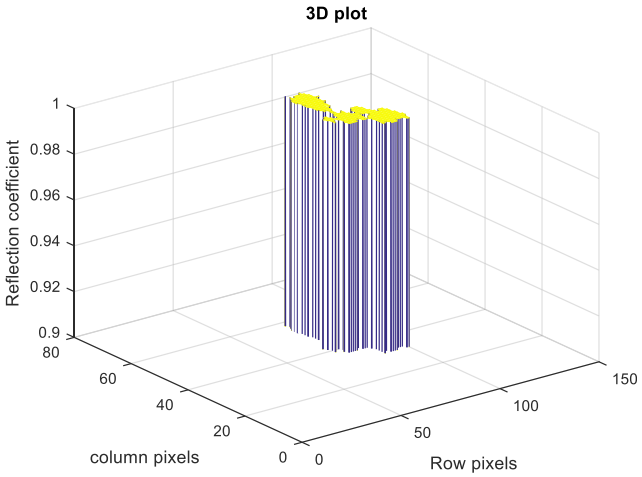

Fig. 19 3D view of the projected microcalcification alone in the RoI with 90° rotation

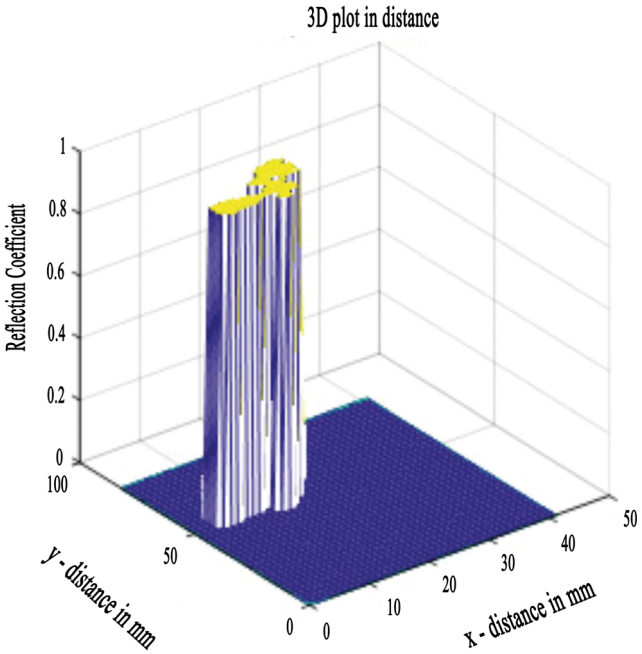

Fig. 18 3D view of projected microcalcification alone in terms of the distance

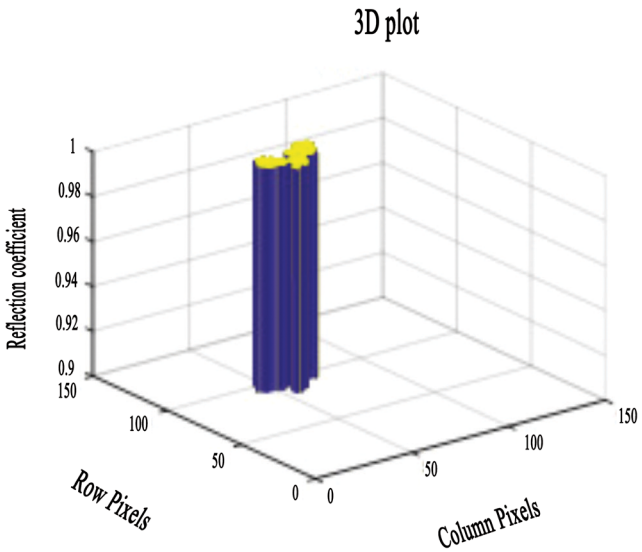

Fig. 20 3D view of the projected microcalcification alone in the RoI with 30° rotation

Table 2 Prediction class to find accuracy

Mammograms	No. of samples	Prediction class			
		TP	FP	TN	FN
Normal	10	–	0	10	–
With malignant microcalcifications	100	99	–	–	1

true negative category. From the calculated mass densities of the considered bins, it could be understood that the radical associated with the abnormal images is calcium phosphate. From the considered unique characteristics, the prediction classes are TP, TN, FP, and FN, and the classification accuracy reaches 99%. In comparison with the existing classification techniques, the proposed methodology gives a very good classification accuracy by using only two physical characteristics of the diagnostic mammograms.

The results obtained are submitted to a clinical doctor for validation and these results are accepted by the physician with a classification accuracy of 99%. The proposed approach is found to be much more effective and efficient compared with the other existing classification approaches that have been used till date. The existing SVM [29], fuzzy [26, 30, 37], and neural network-based classifiers work based on 10 to 15 extracted statistical and textural features [7, 38, 39]. In addition to the size prediction, the proposed algorithm works as a good classifier by only considering two physical characteristics.

Conclusion

This research work proposed a novel automated algorithm using CAD techniques such as binning, calculation of the reflection coefficient and mass density to obtain a 3D view of the projected pattern of the microcalcification using mammograms. From the calculation of the physical characteristics, the occurrence of the microcalcification in a digital mammogram was doubly confirmed. To segment the lesion part effectively, thresholding based on the range of the reflection coefficient was carried out. This method gave a better segmented output than the other existing techniques and size calculation of the malignant lesion in diagnostic mammogram with higher precision. Moreover, from the mass density calculation, it was possible to identify the type of radicals associated with the deposited calcification in the breast tissue. The size calculation of microcalcification was performed by interpolating the intensity in the binned image into the reflection coefficient. Based on that, the lesion part was exactly segmented through the projected 3D view of microcalcification, and its size was exactly calculated. The detection approach utilized in this study focused mainly on the physical characteristics like reflection coefficient and mass density, which are unique, and had not been applied or studied extensively as a part of the result analysis and evaluation in any previous studies. By correlating the reflection coefficient and mass density values of the binned image, the prediction class to categorize the considered mammogram image (malignant and normal) was also achieved with classification accuracy 99%. Thus, the proposed technique is proved as an effective methodology in diagnosing and classifying the abnormalities of the breast cancer with high true positive and true negative results. The 3D view of projected lesion part and their angle rotation is a user-friendly approach, which could be easily understood by radiologists, physician, and even by the patients.

References

1. Tang J, Rangayyan RM, Xu J, El Naqa I, Yang Y: Computer-aided detection and diagnosis of breast cancer with mammography recent advances. IEEE Transactions on Information Technology in Biomedicine 13:236–251, 2009
2. Mudigonda NR, Rangayyan RM, Desautels JL: Detection of breast masses in mammograms by density slicing and texture flow-field analysis. IEEE Trans Med Imaging 20:1215–1227, 2001
3. Kowsalya S, Priyaa DS: An integrated approach for detection of masses and macro calcification in mammogram images using dexterous variant median fuzzy c-means algorithm. In Intelligent Systems and Control (ISCO):10th International Conference, IEEE, 1–10th International Conference, IEEE, 6, 2016
4. Yu S, Guan LA: CAD system for the automatic detection of clustered microcalcifications in digitized mammogram films. IEEE Trans Med Imaging 19:115–126, 2000
5. Ackerman LV, Mucciardi AN, Gose EE: Classification of benign and malignant breast tumors on the basis of 36 radiographic properties. Cancer 31:342–352, 1973
6. Lagzouli M, Elkettani Y: A new morphology algorithm for microcalcifications detection in fuzzy mammograms images. International Journal of Engineering Research & Technology (IJERT):3, 2014
7. Abirami C, Harikumar R, Chakravarthy SS: Performance analysis and detection of micro calcification in digital mammograms using wavelet features. In Wireless Communications, Signal Processing and Networking (WiSPNET), International Conference, IEEE: 2327–2331, 2016
8. Salvado J, Roque B: Detection of calcifications in digital mammograms using wavelet analysis and contrast enhancement. In Intelligent Signal Processing, IEEE International Workshop, IEEE:200–205, 2005
9. Mustra M, Grgic M, Delac K: Enhancement of microcalcifications in digital mammograms. Systems, Signals and Image Processing (IWSSIP), 19th International Conference., IEEE:248–251, 2012
10. Malek AA, Rahman WE, Ibrahim A, Mahmud R, Yasiran SS, Jumaat AK: Region and boundary segmentation of microcalcifications using seed-based region growing and mathematical morphology. Procedia-Social and Behavioral Sciences 8: 634–639, 2010

11. Zhang S, Chen H, Li J: Segmentation of microcalcifications in mammograms based on multi-resolution region growth and image difference. In Image and Signal Processing (CISP), 4th International Congress, IEEE 3:1273–1276, 2011
12. Pradeep N, Girisha H, Sreepathi B, Karibasappa K: Feature extraction of mammograms. International journal of Bioinformatics research 4:241–247, 2012
13. Arai K, Abdullah IN, Okumura H, Kawakami R: Improvement of automated detection method for clustered microcalcification based on wavelet transformation and support vector machine. International Journal of Advanced Research in Artificial Intelligence 2:23–28, 2013
14. Dheeba J, Wiselin Jiji G: Detection of microcalcification clusters in mammograms using neural network. International Journal of Advanced Science and Technology 19, 2010
15. Jemila Rose R, Allwin S: Computerized cancer detection and classification using ultrasound images. International Journal of Engineering Research and Development 5:36–47, 2013
16. Qian Z, Hua G, Cheng C, Tian T, Yun L: Medical images edge detection based on mathematical morphology. Engineering In Medicine And Biology:1–4, 2005
17. Raajan NR, Vijayalakshmi R, Sangeetha S: Analysis of malignant neoplastic using image processing techniques. International Journal of Engineering and Technology 5, 2013
18. Fusco R, Sansone M, Filice S, Carone G, Amato DM, Sansone C, Petrillo A: Pattern recognition approaches for breast cancer DCE-MRI classification: A systematic review. Journal of Medical and Biological Engineering 36:449–459, 2016
19. Roman C, Inglis G, Rutter J: Application of structured light imaging for high resolution mapping of underwater archaeological sites. International Conference on OCEANS, IEEE, 2010
20. Romijn R, Missiaen T, Kinneging N, Blacquière G, vd Brenk S: Archeological site investigation using very high resolution 3D seismics. Proceedings of the Seventh European Conference on Underwater Acoustics, ECUA, 2004
21. Chen S-C: The evolution and future of breast cancer screening—Focus on Asian women. Journal of Medical Ultrasound 23:120–122, 2015
22. Satoto KI, Nurhayati OD, Rizal Isnanto R: Pattern recognition to detect breast cancer thermogram images based on fuzzy inference system method. International Journal of Computer Science and Technology 2:484–487, 2011
23. Makandar A, Halalli B: Breast cancer image enhancement using median filter and CLAHE. International Journal of Scientific & Engineering Research 6:462–465, 2015
24. Jothilakshmi GR, Gopinathan E: Mammogram enhancement using quadratic adaptive volterra filter—A comparative analysis in spatial and frequency domain. ARPN Journal of Engineering and Applied Sciences 10:5512–5517, 2015
25. Al-Bayati M, El-Zaart A: Mammogram images thresholding for breast cancer detection using different thresholding methods. Advances in Breast Cancer Research 2:72–77, 2013
26. Akila K, Sumathy P: Early breast cancer tumor detection on mammogram images. International Journal of Computer Science and Engineering Technology 5:334–336, 2015
27. Jothilakshmi GR, Sharmila P, Raaza A: Mammogram segmentation using region based method with split and merge technique. Indian Journal of Science and Technology 9:1–6, 2016
28. Schaefer G, Zavisek M, Nakashima T: Thermography based breast cancer analysis using statistical features and fuzzy classification. Pattern Recognition 42:1133–1137, 2009
29. Kourou TPE, Exarchos KP, Karamouzis MV, Fotiadis DI: Machine learning applications in cancer prognosis and prediction. Computational and structural biotechnology journal 13:8–17, 2015
30. Tintu PB, Paulin R: Detect breast cancer using fuzzy C means techniques in Wisconsin prognostic breast cancer (WPBC) data sets. International Journal of Computer Applications Technology and Research 2:614–617, 2013
31. Scott R, Kendall C, Stone N, Rogers K: Elemental vs. phase composition of breast calcifications. Scientific Reports 7:136–142, 2017
32. Martini N: Modeling of the calcium/phosphorus mass ratio for breast imaging. Journal of Physics: Conference Series 633, 2015
33. Cracoviensia, Folia Medica: Chemical composition and morphology of renal stones. Folia medica Cracoviensia 53:5–15, 2013
34. Sabudin SALINA: In vitro bioactivity of macroporous calcium phosphate scaffold for biomedical application. Key Engineering Materials Trans Tech Publications:705, 2016
35. Ciecholewski M: Microcalcification segmentation from mammograms: A morphological approach. Journal of Digital Imaging 30:172–184, 2017
36. khehra B s, pharwaha A p s: Classification of clustered microcalcifications using MLFFBP-ANN and SVM. Egyptian Informatics journal 17:11–20, 2016
37. Kumar M, Thakkar VM, Bhatt U, Soliyal N: Detection of suspicious lesions in mammogram using fuzzy C-means algorithm. In Advances in Computing, Communications and Informatics (ICACCI), International Conference, IEEE:1553–1557, 2016
38. Pradeep N, Girisha H, Sreepathi B, Karibasappa K: Feature extraction of mammograms. International journal of Bioinformatics research 4:241–248, 2012
39. Fathima MM, Manimegalai D, Thaiyalnayaki S: Automatic detection of tumor subtype in mammograms based on GLCM and DWT features using SVM. In Information Communication and Embedded Systems (ICICES), International Conference IEEE:809–813, 2013